

Supportting information

Controlled synthesis of cobalt-organic framework:

hierarchical micro/nanospheres for high-performance supercapacitors

Xinxin Hang*, Yadan Xue, Meng Du, Rui Yang, Jiawei Zhao, Huan Pang*

School of Chemistry and Chemical Engineering, Institute for Innovative Materials and Energy,

Yangzhou University, Yangzhou, 225002, Jiangsu, P. R. China.

E-mail: hangxinxin@yzu.edu.cn (X. Hang); huanpangchem@hotmail.com (H. Pang)

Experimental Section

Materials and Characterizations. All reagents were purchased from commercial sources and used as received. Morphologies of the samples were observed by field emission scanning electron microscopy (FESEM, Zeiss-Supra55). Transmission electron microscopic (TEM) and high-angle annular dark-field scanning transmission electron microscopic (HAADF-STEM) images were collected on a Tecnai G2 F30 S-TWIN transmission electron microscopy. Power X-ray diffraction (PXRD) measurements were performed on a Bruker D8 Advanced X-ray diffractometer (CuK α radiation: $\lambda = 0.15406$ nm). Fourier transform-infrared (FT-IR) spectra were recorded on a BRUKEREQUINOX-55 IR spectrophotometer. X-ray photoelectron spectroscopy (XPS) analyses were measured on ESCALAB 250Xi, equipped with a standard monochromatic Al-K α source ($h\nu = 1486.6$ eV) a monochromatic AlK α excitation under vacuum higher than 1×10^{-7} Pa. Inductively coupled plasma-atomic emission spectrometer (ICP-AES) elemental analysis were collected on an Elan DRC-e Plasma mass spectrometer. All electrochemical measurements were performed on the CHI660e and CHI760e instrument.

Synthesis of Co-MOF/M1. Co-MOF/M1 was obtained from solvothermal reaction of the mixture of CoCl $_2$ ·6H $_2$ O (95.172 mg, 0.4 mmol), pyridine-3,5-dicarboxylic acid (H $_2$ pdc, 13.36 mg, 0.08 mmol), N, N-dimethylformamide (DMF, 5 ml) and methanol (MeOH, 5 ml) in a 25 ml Teflon-lined autoclave which was kept at 120 °C for 72 h, and then cooled to room temperature. The purple powder was collected, which were washed with MeOH and dried in air.

Synthesis of Co-MOF/M2. Co-MOF/M2 was obtained under the same reaction like Co-MOF/M1 except $\text{CoCl}_2 \cdot 6\text{H}_2\text{O}$ (47.586 mg, 0.2 mmol) and H_2pdc (6.68 mg, 0.04 mmol) were used.

Synthesis of Co-MOF/M3. Co-MOF/M3 was obtained under the same reaction like Co-MOF/M1 except $\text{CoCl}_2 \cdot 6\text{H}_2\text{O}$ (23.793 mg, 0.1 mmol) and H_2pdc (3.34 mg, 0.02 mmol) were used.

Electrochemical measurements

Supercapacitors

The electrochemical measurement of supercapacitors was performed on CHI660e working station in 3.0 M KOH solution at room temperature. Cyclic voltammetry (CV), Galvanostatic charge-discharge (GCD) and electrochemical impedance spectroscopy (EIS) were used to investigate the capacitive properties of Co-MOF/M1, Co-MOF/M2 and Co-MOF/M3. The EIS measurements were conducted in the frequency range of 100 kHz to 0.1 Hz at the open-circuit voltage.

For the three-electrode cell, the working electrode was fabricated by mixing the active materials (Co-MOF/M1 or Co-MOF/M2 or Co-MOF/M3), acetylene black, and polytetrafluoroethylene at a mass ratio of 80 : 15 : 5. The slurry was coated on a piece of nickel foam ($\approx 1 \text{ cm}^2$), which was then pressed into a thin foil at a pressure of 10 MPa. The typical mass loading of the electrode material was 1.0 mg. A platinum electrode and a Hg/HgO electrode served as the counter and reference electrode, respectively.

For the two-electrode cell, Co-MOF/M1 (Co-MOF/M2 or Co-MOF/M3) and

activated carbon (AC) were used as positive electrode and negative electrode, respectively. The positive and negative electrodes were fabricated by mixing Co-MOF/M1 (Co-MOF/M2 or Co-MOF/M3) //AC, acetylene black and polytetrafluoroethylene at a weight ratio of 80 : 15 : 5. The slurry was coated on a piece of nickel foam ($\approx 1 \text{ cm}^2$), which was then pressed into a thin foil at a pressure of 10 MPa.

Calculations

The specific capacitance of the electrode material was calculated from the charge-discharge curves according to the equation:

$$C = Q / (m \times \Delta V) = \int Idt / (m \times \Delta V) = I \times t_{\text{discharge}} / (m \times \Delta V) \quad \text{equation S1}$$

Where m is the weight of the electrode materials, I is the discharge current, $t_{\text{discharge}}$ is discharge time, ΔV is the potential drop during discharge (excluding the IR drop).

The voltammetric response of an electrode at various sweep rates can be generally expressed as:

$$i = a\nu^b \quad \text{equation S2}$$

The logarithm of both anodic and cathodic peak currents (i) were plotted against the logarithm of scan rate (ν) to obtain the slope as fitted parameter b .

$$\log i = \log a + b \log \nu \quad \text{equation S3}$$

where i is the maxima of current densities (A g^{-1}), ν is the scan rate (mV s^{-1}), and a and b are arbitrary coefficients. The value of b can be calculated from the linear plots as the slop.

The dependency of the voltammetric sweep rate on the current response was

investigated to quantitatively resolve the contribution from capacitive and diffusion-controlled processes. Diffusion and capacitive contribution to the current response can be analyzed as follow:

$$i(V) = k_1v + k_2v^{1/2} \quad \text{equation S4}$$

which can be rearranged as:

$$i(V)/v^{1/2} = k_1v^{1/2} + k_2 \quad \text{equation S5}$$

where i , V and v refer to the current density ($A\ g^{-1}$), potential (V) and scan rate ($V\ s^{-1}$), respectively. The k_1 and k_2 are adjustable parameters. The voltage profile for the capacitive current is compared to the total current obtained scan rates from 10 to 100 $mV\ s^{-1}$. By linear fitting, values of k_1 and k_2 could be calculated under potentials from 0 to 0.6 V. The current contributions from capacitive process (k_1v) and from diffusion-controlled ($k_2v^{1/2}$) redox process can be identified.

Supplementary data

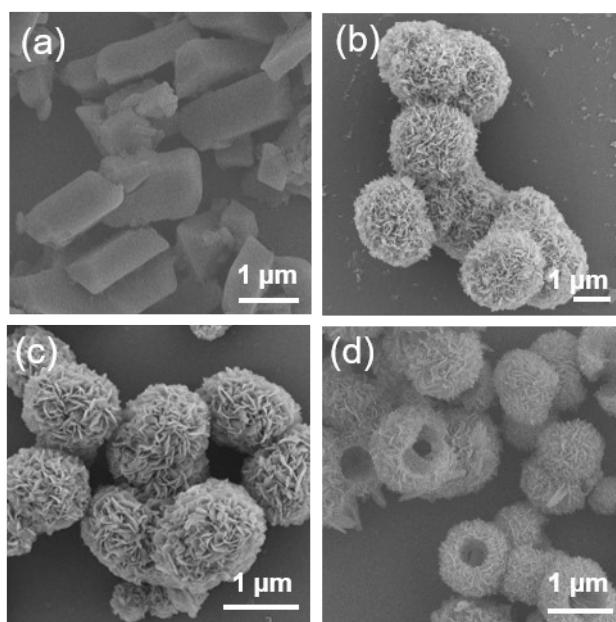


Figure S1. SEM of Co-MOF (a), Co-MOF/M1 (b), Co-MOF/M2 (c) and Co-MOF/M3 (d).

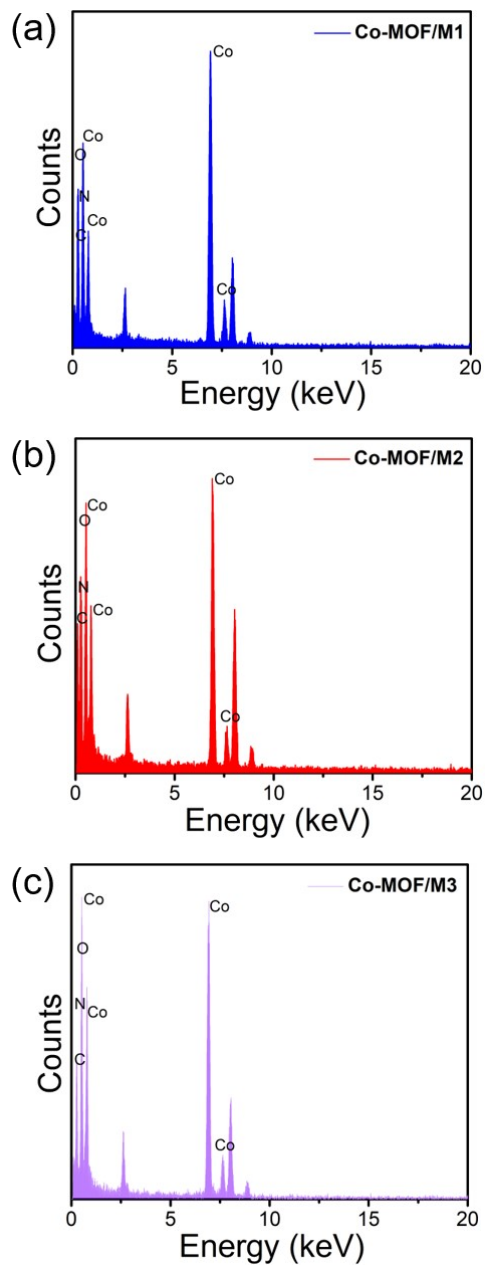


Figure S2. EDS analysis of Co, O, N and C elements in Co-MOF/M1 (a), Co-MOF/M2 (b) and Co-MOF/M3 (c).

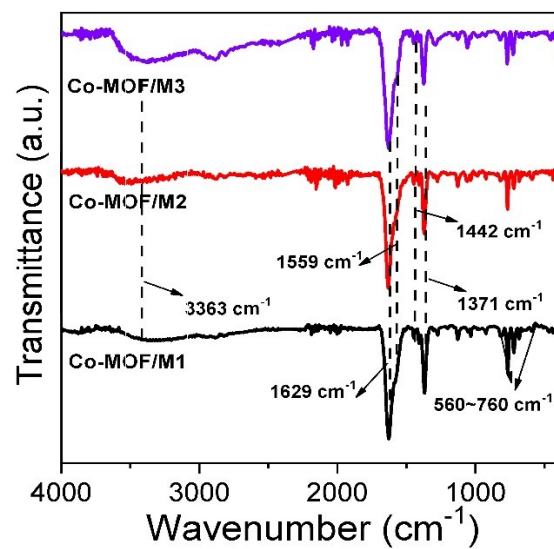


Figure S3. FT-IR patterns of Co-MOF/M1, Co-MOF/M2 and Co-MOF/M3.

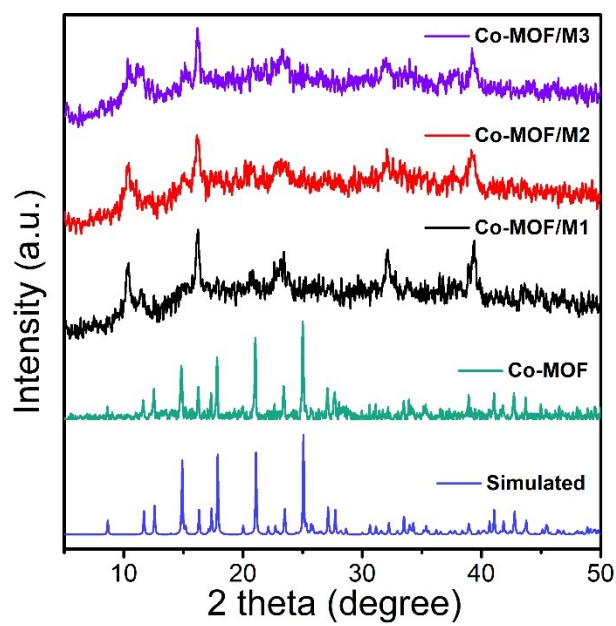


Figure S4. XRD patterns of Co-MOF, Co-MOF/M1, Co-MOF/M2 and Co-MOF/M3.

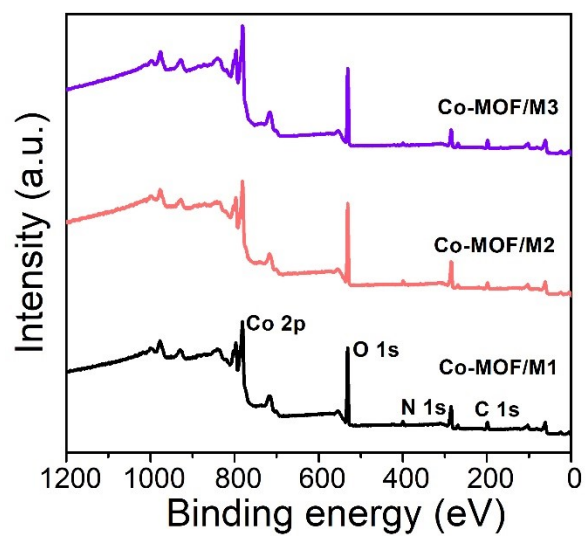


Figure S5. XPS spectra: survey scan of Co-MOF/M1, Co-MOF/M2 and Co-MOF/M3.

Table S1. ICP-AES analyses of Co-MOF/M1, Co-MOF/M2 and Co-MOF/M3.

Sample	Co ²⁺ used (wt%)	Co ²⁺ detected (wt%)
Co-MOF/M1	21.72	21.43
Co-MOF/M2	21.72	22.61
Co-MOF/M3	21.72	22.56

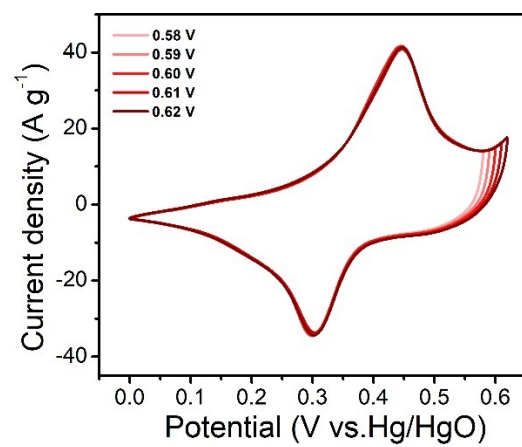
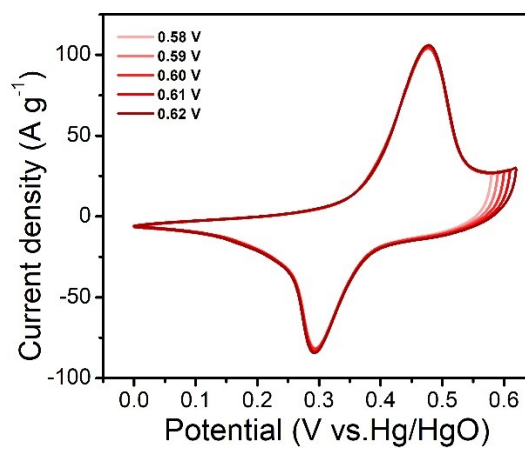
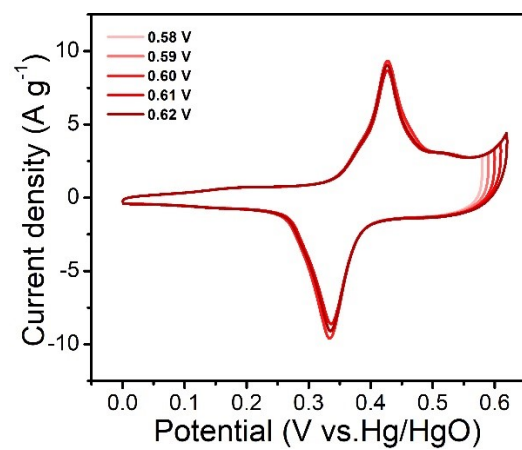


Figure S6. CV curves of Co-MOF/M1, Co-MOF/M2 and Co-MOF/M3 electrodes under different voltages.

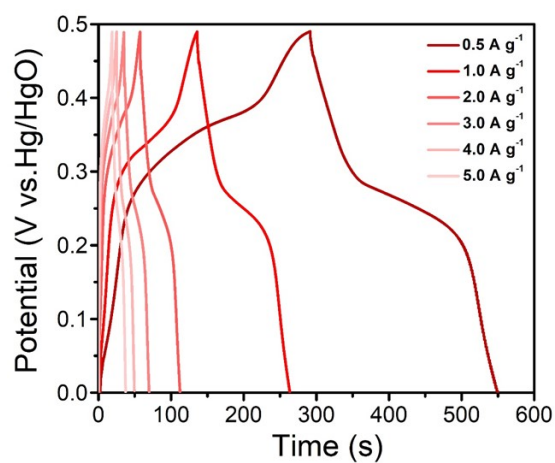
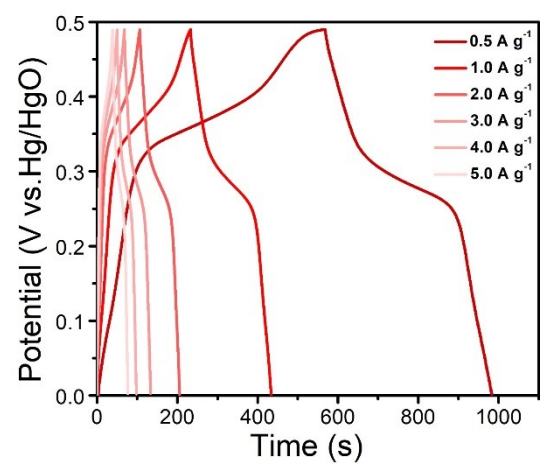
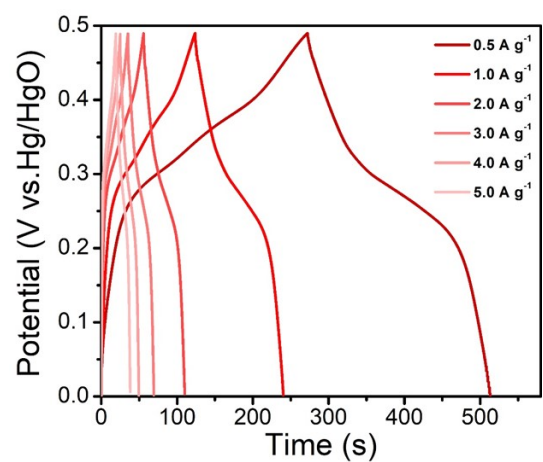


Figure S7. GCD profiles of Co-MOF/M1, Co-MOF/M2 and Co-MOF/M3 electrodes at different current densities.

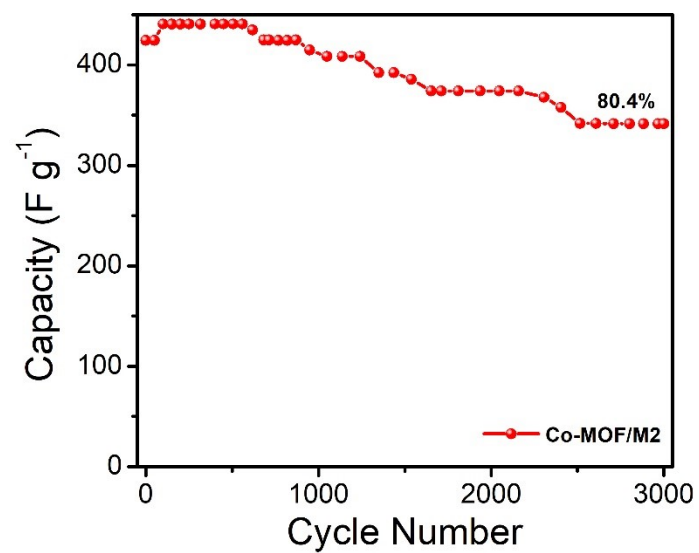


Figure S8. Long-term cycling performance of Co-MOF/M2 at a current density of 5 A g^{-1} .

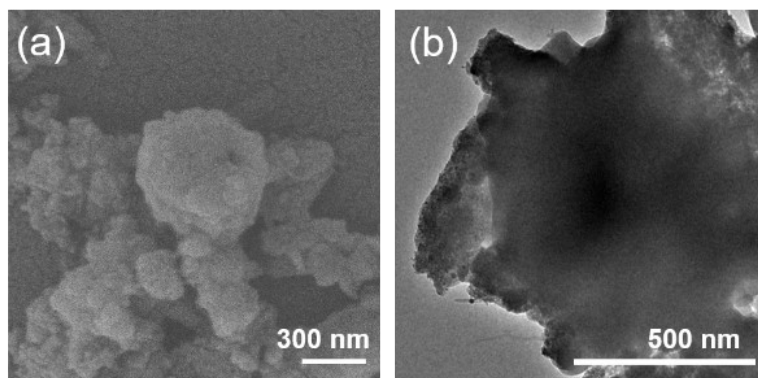


Figure S9. (a) SEM image and (b) TEM image of Co-MOF/M2 electrode after cycling stability tests.

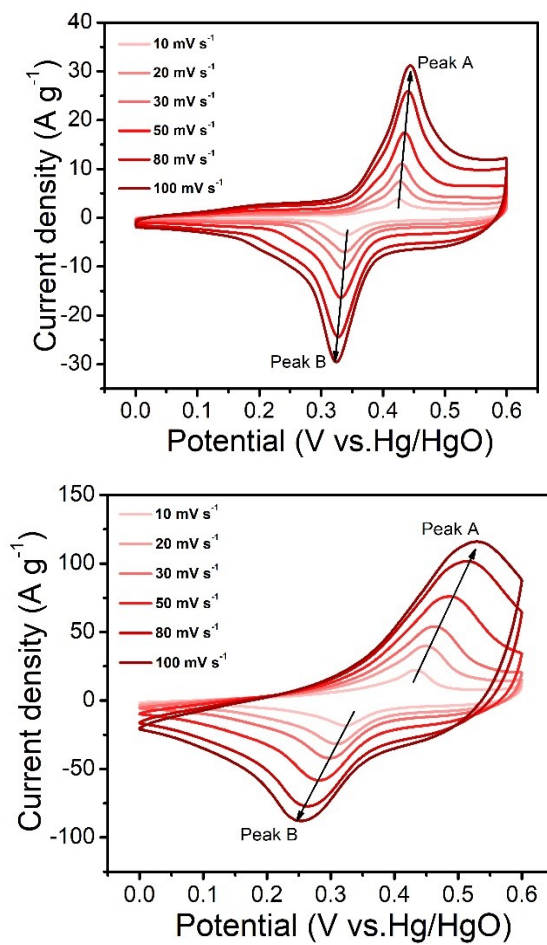


Figure S10. CV curves of Co-MOF/M1 and Co-MOF/M3 electrodes at different scan rates.

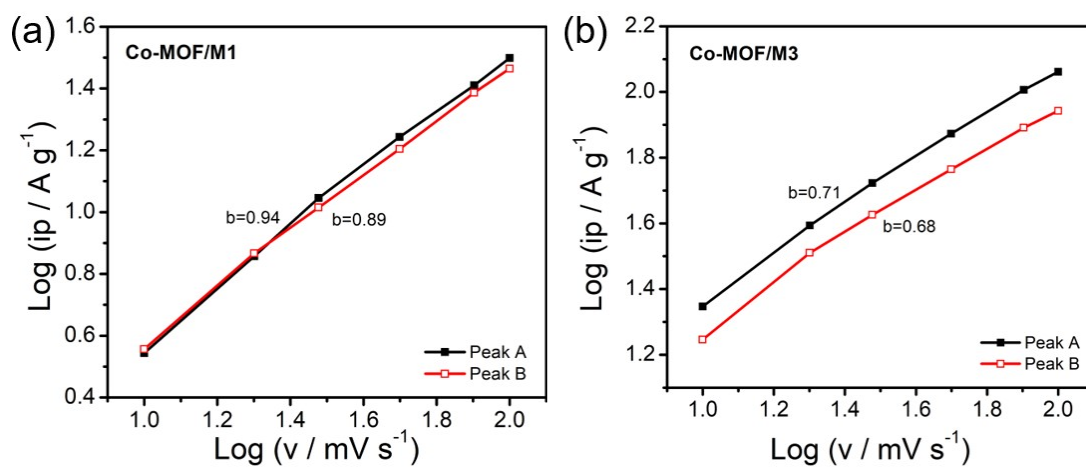


Figure S11. Calculation of the b values for Co-MOF/M1 and Co-MOF/M3.

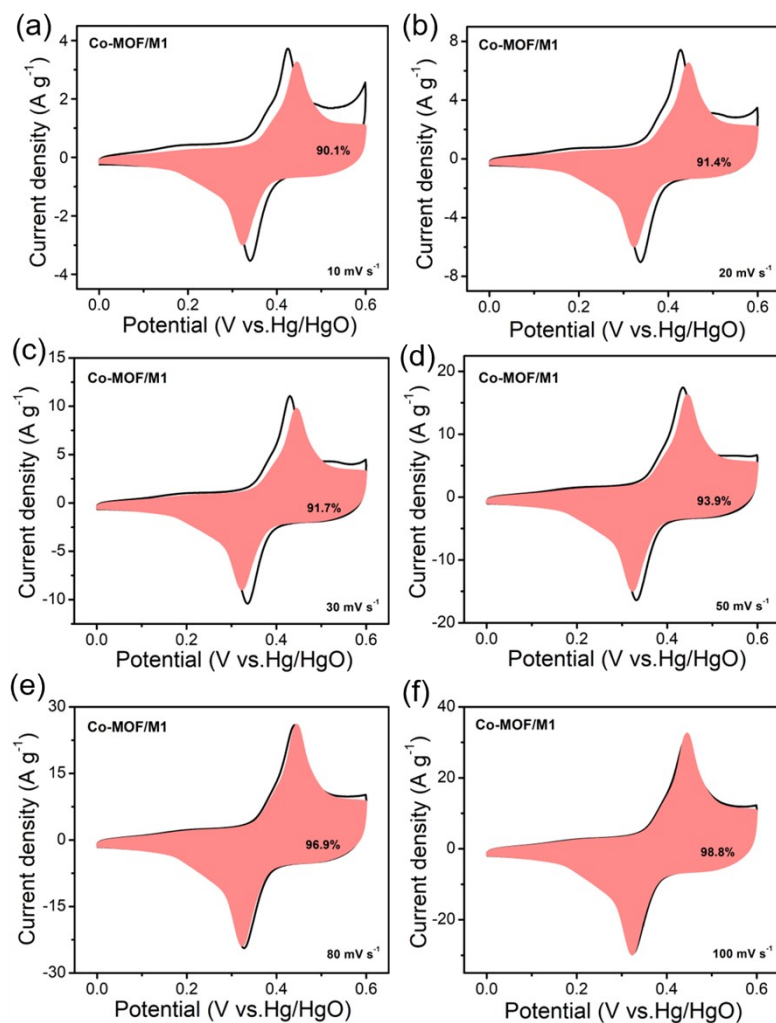


Figure S12. CV curves of Co-MOF/M1 with separation between total current (black line) and capacitive currents (red shadow) at (a) 10, (b) 20, (c) 30, (d) 50, (e) 80 and (f) 100 mV s⁻¹ in 3.0 M KOH.

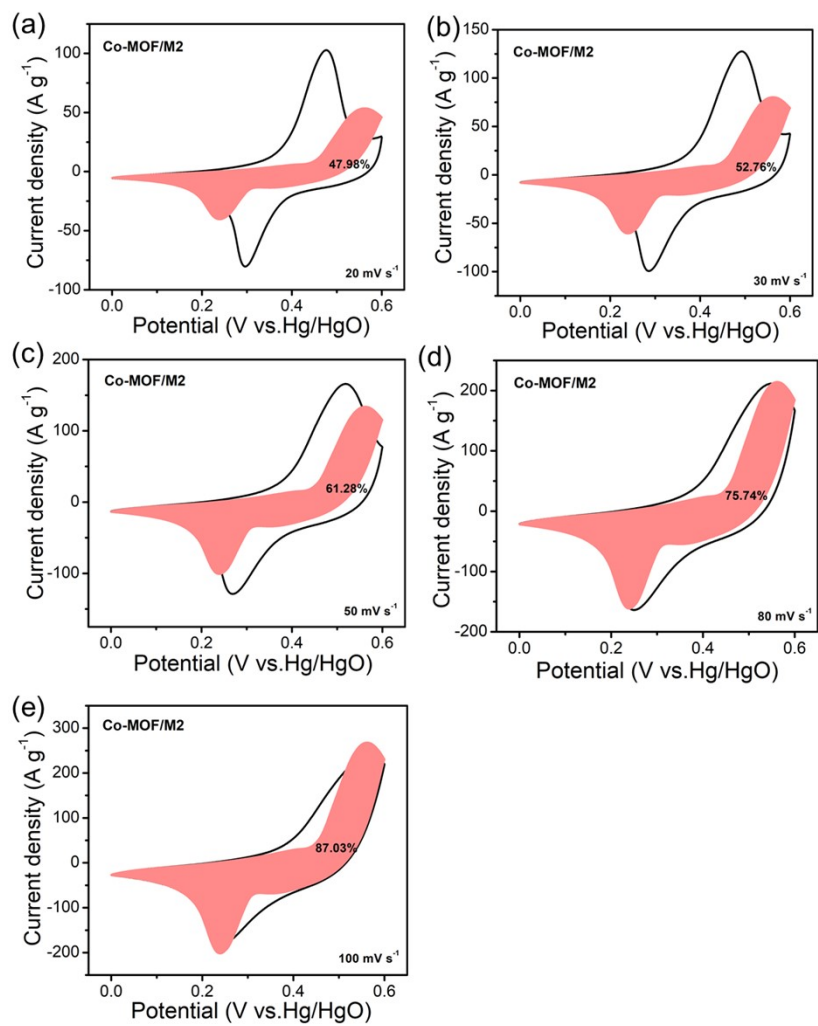


Figure S13. CV curves of Co-MOF/M2 with separation between total current (black line) and capacitive currents (red shadow) at (a) 20, (b) 30, (c) 50, (d) 80 and (e) 100 mV s⁻¹ in 3.0 M KOH.

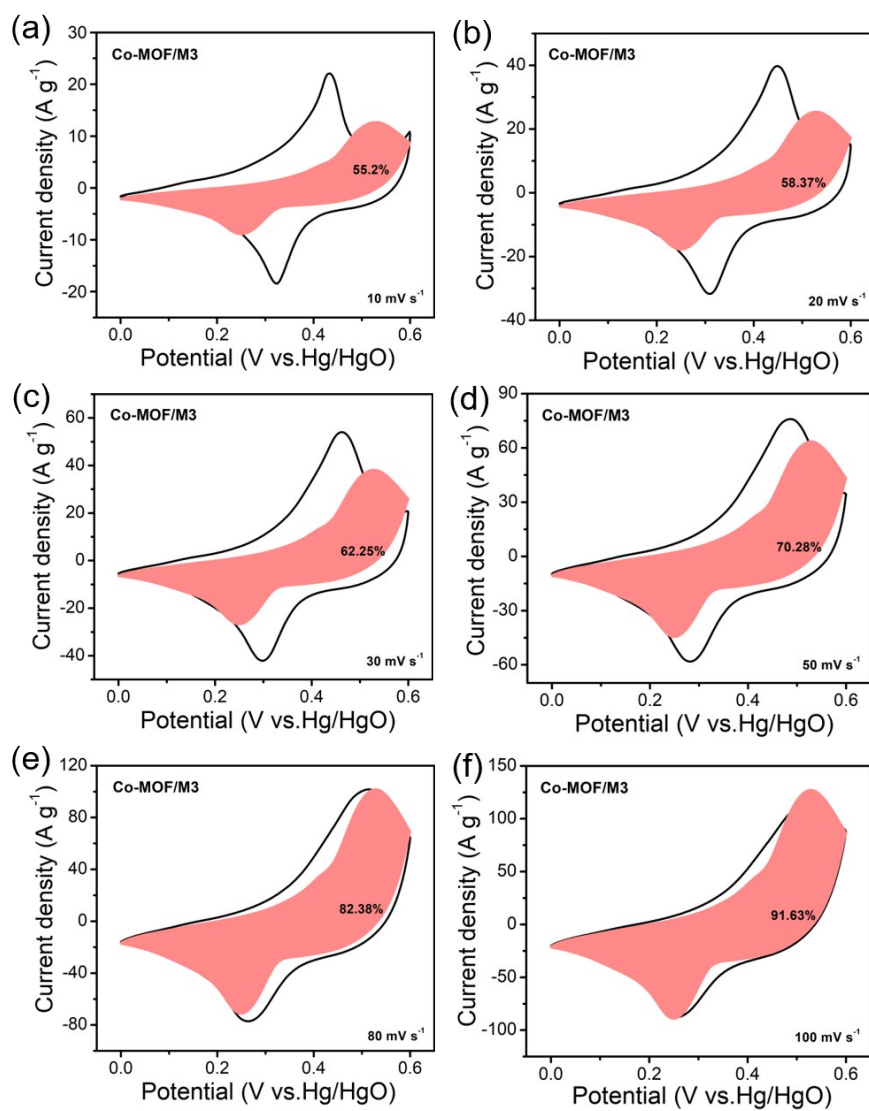


Figure S14. CV curves of Co-MOF/M3 with separation between total current (black line) and capacitive currents (red shadow) at (a) 10, (b) 20, (c) 30, (d) 50, (e) 80 and (f) 100 mV s⁻¹ in 3.0 M KOH.

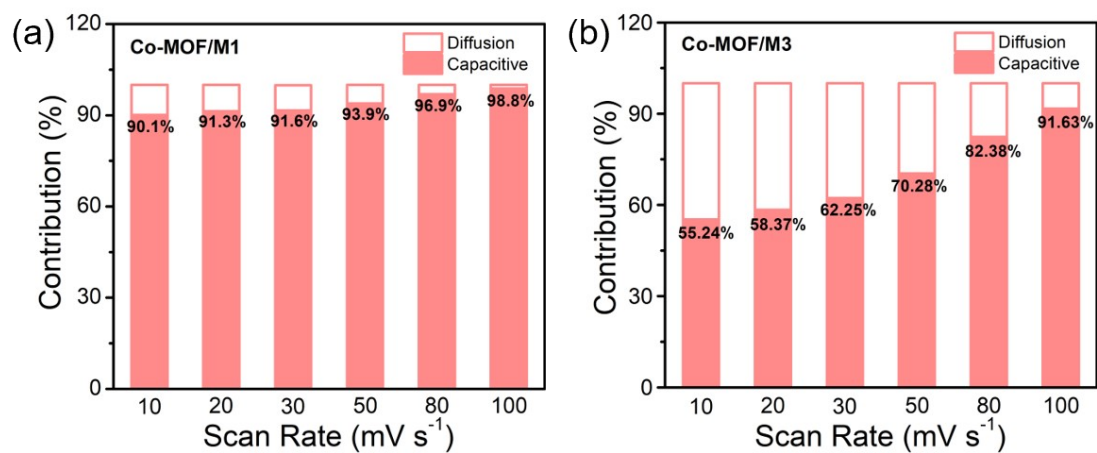


Figure S15. Capacitive contributions of Co-MOF/M1, Co-MOF/M2 and Co-MOF/M3 at different scan rates.

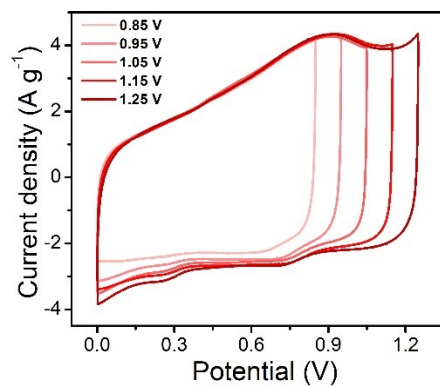


Figure S16. CV curves of Co-MOF/M2//AC in different potential windows.

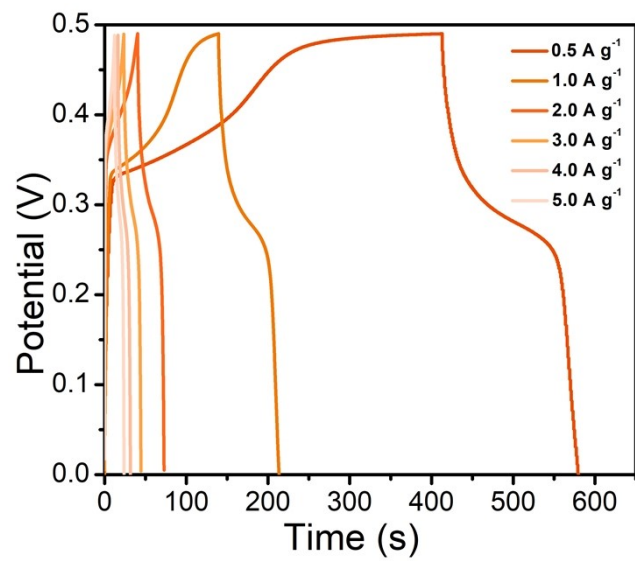


Figure S17. GCD profiles of AC electrode at different current densities.

Table S2. Comparisons of supercapacitor performance of recently reported cobalt-based materials with Co-MOF/M2 in this work.

Sample	Electrolyte (KOH, M)	Specific capacity, F g ⁻¹ (low current density, A g ⁻¹)	Specific capacity, F g ⁻¹ (high current density, A g ⁻¹)	Ref.
Co(OH) ₂ nanocone arrays	2	562 (2.0)	385 (16.0)	1
Co ₃ O ₄ microdumbbell	3	407 (1.0)	319 (6.0)	2
[Me ₂ NH ₂][Co ₃ (OH)(L) ₂ (H ₂ O) ₃]·6H ₂ O	3	300 (1.0)	106 (5.0)	3
Co-NC3	3	310 (0.5)	115 (5.0)	4
Co-MOF	3	240 (1.0)	90 (10.0)	5
COP	3	274 (0.5)	227.3 (5.0)	6
Co-BTB-I-450	3	342.1 (0.5)	280.3 (5.0)	7
Co-MOF/210	3	495.6 (0.25)	340 (5.0)	8
Co-MOF-140-1:2	3	414.5 (0.5)	104 (10.0)	9
Co-MOF _{6h}	3	450.89 (0.5)	299 (5.0)	10
Co-MOF/M2	3	430 (0.5)	398 (5.0)	This work

References

1. Cao, F.; Pan, G. X.; Tang, P. S.; Chen, H. F. Hydrothermal-synthesized Co(OH)₂ nanocone arrays for supercapacitor application. *J. Power Sources* **2012**, *216*, 395–399.
2. Dam, D. T.; Lee, J. -M. Three-dimensional cobalt oxide microstructures with brush-like morphology via surfactant-dependent assembly. *ACS Appl. Mater. Interfaces* **2014**, *6*, 20729–20737.
3. Ghosh, S.; Maity, C. K.; Nayak, G.C.; Nayek, H. P. A cobalt(II) metal-organic framework featuring supercapacitor application. *J. Solid State Chem.* **2020**, *282*, 121093.
4. Devi, B.; Jain, A.; Roy, B.; Rao R, B.; Tummuru, N. R.; Halder, A.; Koner, R. R. Cobalt-embedded N-doped carbon nanostructures for oxygen reduction and supercapacitor applications. *ACS Appl. Nano Mater.* **2020**, *3*, 6354–6366.
5. Yu, H. N.; Xia, H. C.; Zhang, J. N.; He, J.; Guo, S. Y.; Xu, Q. Fabrication of Fe-doped Co-MOF with mesoporous structure for the optimization of supercapacitor performances. *Chin. Chem. Lett.* **2018**, *29*, 834–836.
6. Jing, Q. L.; Li, W. T.; Wang, J. J.; Chen, X. D.; Pang, H. Calcination activation of three-dimensional cobalt organic phosphate nanoflake assemblies for supercapacitors. *Inorg. Chem. Front.* **2021**, *8*, 4222–4229.
7. Zhu, Z. Y.; Han, C.; Li, T. T.; Hu, Y.; Qian, J. J.; Huang, S. M. MOF-templated syntheses of porous Co₃O₄ hollow spheres and micro-flowers for enhanced performance in supercapacitors. *CrystEngComm* **2018**, *20*, 3812.
8. Xuan, W. L.; Ramachandran, R.; Zhao, C. H.; Wang, F. Influence of synthesis temperature on cobalt metal-organic framework (Co-MOF) formation and its electrochemical performance towards supercapacitor electrodes. *J. Solid State Electr.* **2018**, *22*, 3873–3881.
9. Shao, D. N.; Wang, L.; Lu, B.; Guo, J. Y.; Zhang, S. Y.; Lu, Y. A high N content cobalt-based metal organic framework with nanorod structure for supercapacitor electrode material. *J. Electroanal. Chem.* **2019**, *847*, 113188.
10. Wang, Z. K.; Chen, J. Q.; Bi, R.; Dou, W.; Wang, K. B.; Mao, F. F.; Wu, H.;

Wang, S. S. Supercapacitor and oxygen evolution reaction performances based on morphology-dependent Co-MOFs. *J. Solid State Chem.* **2020**, 283, 121128.